PROCEEDINGS, 43rd Workshop on Geothermal Reservoir Engineering
Stanford University, Stanford, California, February 12-14, 2018
SGP-TR-213

Hydrothermal Spallation Of Barre Granite Using Supercritical Water Jets

Ivan Beentjes, Jay T. Bender, Sean D. Hillson, and Jefferson W. Tester

2160 Snee Hall, Cornell University, Ithaca, NY 14853

ib283@cornell.edu

Keywords: spallation, comminution, supercritical water, hydrothermal jet, advanced drilling, geothermal drilling, chemical enhanced drilling, chemical drilling.

ABSTRACT

Hydrothermal spallation drilling addresses some of the limitations encountered in flame-jet spallation drilling. In particular, it enables drilling in aqueous media at the high borehole pressures encountered in deep geothermal drilling. In this study, an electrically heated hydrothermal jet was impinged on the surface of cylindrical Barre Granite samples (basement rock) contained in a hydrothermal autoclave reactor. Comminution of the rock samples' surface was achieved at supercritical water temperatures ranging from 535°C to 560°C in a 22.5-27 MPa pressure environment to simulate deep wellbore conditions. Preferential removal of quartz grains from the rock matrix was observed.

In the cases examined experimentally, it was found that comminution cannot be attributed to erosion by either the jet's momentum, or by differential pressure forces. Additionally, the rate of silica removal was greater than can be attributed to dissolution alone, implying a secondary comminution mechanism associated with hydrothermal spallation. However, experimentally determined heat flux and surface temperature measurements indicated that hydrothermal comminution occurred below the empirically determined minimums for the onset of continuous thermal spallation, from low density flame jets or laser heating at atmospheric conditions in air. Successful chemically enhanced hydrothermal spallation drilling experiments reduced the temperature and heat flux threshold for spallation. In these tests sodium hydroxide was introduced into the hydrothermal jet to weaken the rock matrix by increasing the dissolution rates of the constituent minerals.

1. INTRODUCTION

Currently fossil fuels provide the majority of society's energy needs, but they are a finite, non-renewable energy source, and one of the main producers of anthropogenic carbon emissions. To address these challenges, alternative, low carbon energy sources should be developed to assist in meeting global energy demand in a sustainable manner. However, a major drawback of some renewable energy solutions (such as wind and solar) is that they produce power intermittently, thereby creating a need for storage and for electrical power generation sources that can follow varying demand with relatively rapid response time (i.e., dispatchable). Electrical power generation using renewable geothermal resources is fully dispatchable and available with high capacity factors (Tester, et al., 2006). Additionally, rather than having to convert the thermal energy contained in a geothermal resource to electricity it can be used directly to heat buildings, provide hot water, and to meet heating needs for many commercial processes which globally represents over 56% (49 EJ) and 45% (13.7 EJ) of the annual residential and commercial energy consumption respectively (Ürge-Vorsatz, et al., 2015), or 8.4 EJ residential and 3.7 EJ commercial in the U.S. (Fox, et al., 2011).

Presently, geothermal development has been primarily focused on moderate to high grade resources where surface expressions, knowledge of a region's structural geology, and geophysical and geochemical measurements provide a basis for locating hydrothermal fluids at relatively shallow depths (< 4 km). In principle, sufficiently high temperature geothermal formations can be found anywhere on earth with a well of sufficient depth by utilizing a set of technologies associated with Enhanced Geothermal Systems (EGS) (Tester, et al., 2006) (Blackwell, et al., 2011). A major obstacle limiting wider adoption of EGS is that lower grade formations must be used requiring deeper, more challenging drilling to reach depths with adequate temperatures resulting in higher technical risks and costs. These difficulties include, but are not limited to, the hardness and competency of the constituent rocks, extreme wellbore depths and pressures, and the presence of corrosive salts and ions in aqueous media (Finger & Blankenship, 2010), all of which significantly shorten the lifespan of conventional rotary drill bits and increase risks (Macini & Mesini, 1994). Compounding these problems is drill bit wear, which requires the entire drill string be removed from the well to replace the bit – using a process called tripping. Tripping time increases with well depth adding significant costs when drilling deep wells (> 4 km). Furthermore, in hard basement rock formations, bit wear rates increase leading to more frequent tripping. Alternative drilling techniques that can avoid excessive bit wear would lower costs, reduce risks and well drilling times and therefore greatly improve the economic viability of geothermal energy development.

Thermal spallation drilling is such a method by which favorable rock formations can be penetrated at fairly high rates with minimal drill string wear because there is no direct contact between the bottom hole assembly and the rock (Rauenzahn & Tester, 1985) (Williams, 1986) (Rauenzahn & Tester, 1989). In thermal spallation a high temperature jet imposes a very high heat flux (0.03 – 0.3 kW/cm^2), resulting in a steep thermal gradient perpendicular to the rock surface producing thermal stresses sufficient to induce fracture growth near the rock surface. The induced thermal stress is superimposed on residual internal stresses leading to tensile failure and spall formation, Figure 1A. Any dislocations, voids, and micro-fractures coalesce into larger fractures, which increase the local thermal contact resistance limiting heat transfer farther into the rock. This resistance increases the localized temperature and resultant thermal

stresses, Figure 1B. The locally heated rock surface then expands against the cooler surrounding rock, and failure occurs when the confining stresses force the thermally expanding rock surface to buckle, violently ejecting the chip from the surface, Figure 1C. If the heat flux at the rock surface is too low, the heat transferred to the rock will dissipate, allowing the rock to expand at a rate that does not force spallation.

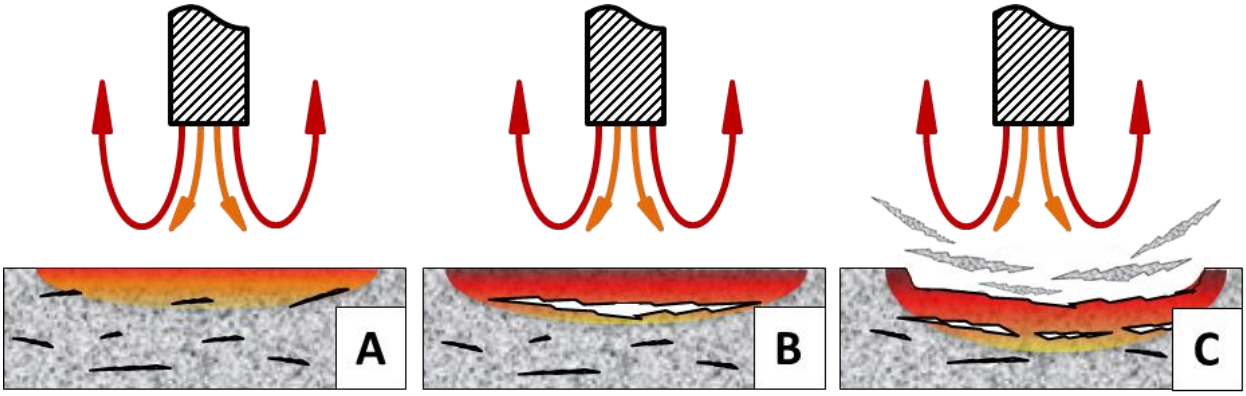

Figure 1: The thermal spallation process. A. Heat applied to the rock propagates small fractures. B. These fractures combine into significant cracks. C. The increased heating results in spalls being ejected from the rock surface while new fractures are formed.

Thermal spallation drilling in low density air environments has been demonstrated in field tests to drill about three times faster than conventional rotary drills to depths of 300 meters in hard quartz-bearing igneous rocks such as granite (Browning, 1981) (Wilkinson & Tester, 1993). Spallation has the potential in suitable stable rock formations to allow the entire well drilling operation to proceed continuously without bit replacement. Drill-string trips would only be needed when casing is installed. With higher penetration rates and fewer trips, the duration of the drilling operation can be reduced considerably. Cost savings result from lower rig rental charges and the elimination costs associated with bit replacement although some operational and equipment costs like fuel, pumps, and compressors may be higher. As a result, spallation drilling costs could potentially be much lower than conventional rotary drilling particularly for deep geothermal wells (> 3 km).

A challenge with adapting the thermal spallation drilling technique for EGS resources is that very deep wellbores will require a drilling fluid to stabilize the borehole and assist with lifting comminuted rock spalls. Thermal spallation field drilling operations to date have been limited to depths of less than 1000m and have typically relied on a high velocity gas flame at near atmospheric pressures comparable to percussion drilling in open, air filled boreholes. In response to this potential limitation, research into hydrothermal flames has shown that they can be produced under the conditions found in fluid-filled boreholes (Stathopoulos, 2014) (Augustine, 2009). Nonetheless, there are multiple obstacles associated with hydrothermal flame jet drilling to overcome for real-world implementation including, flame extinguishment, flame (re)ignition, flame jet penetration length into a cooler co-axial flow, delivery of gaseous oxidant downhole, etc.. Earlier research indicates that it may be possible to achieve the conditions necessary for spallation without the use of flames, and instead employ a supercritical water jet to attain the desired surface temperature (~450°C) and heat flux conditions (~0.5 MW/m^2) at the rock surface. (Wilkinson & Tester, 1993) (Williams, et al., 1988). A significant difference between these hydrothermal jet spallation experiments and flame jet spallation (using combustion) is the high pressure and high fluid density environment surrounding the rock sample. In 2008, Potter Drilling achieved hydrothermal jet spallation of Sierra White Granite, at a jet temperature of 700°C (Potter Drilling, 2008).

These preliminary findings motivated the current study to characterize and improve the understanding of underlying differences between flame and hydrothermal jet spallation. The initial experimental objective of this study was to quantify a low temperature limit for a hydrothermal jet to induce spallation in a high pressure supercritical water environment comparable to what would be encountered in a deep EGS borehole. The approach taken used a modified bench scale hydrothermal apparatus to expose Barre Granite rock samples to a supercritical water jet over a range of temperature and pressure conditions (530-550°C, 22.5-28 MPa).

2. HYDROTHERMAL SPALLATION REACTOR

A high temperature and pressure spallation reactor capable of delivering a hydrothermal jet of supercritical deionized water up to 600°C and 31 MPa based on an original design of Jared Potter was modified at the Cornell Energy Institute over a 5-year period (Hillson & Tester, 2015). Pure deionized water was used for the hydrothermal jet and heated by a series of electrical heaters totaling 14.8 kW (Augustine, 2009), with approximately 94 percent of this available energy delivered to the exiting fluid jet before it impinges upon the rock face. The main reactor accommodates a 2.54 cm diameter, 8 cm long cylindrical Barre Granite rock sample, and has a cap fitted with sealing O-rings that allow the jet to impinge directly on the rock surface in an isolated environment; see Figure 2B. The reactor is contained within a larger pressure vessel that is limited to a maximum temperature of 80°C to ensure safe operation. See Figure 3 for a complete piping diagram of the experimental system.

While pressurized water is being heated to the desired supercritical temperature, the reactor is positioned in the lower (cooler) part of the pressure vessel, so that the rock sample remains in fluid at a temperature less than 80°C. Holding the sample at this lower temperature avoids thermal expansion due to gradual heating which would occur if the sample were located closer to the hydrothermal jet.

To perform a comminution experiment at a desired jet temperature, the granite sample is raised under pressure from the lower part of the containment vessel to the top where the hydrothermal jet impinges on its top surface. A cooling water jacket envelops the remaining sides of the rock sample, see Figure 2C, to keep the bulk sample cooler. The external cooling water jacket counteracts the intense heating by the hydrothermal jet, thereby limiting the tendency of the small rock sample to relieve stress through thermal expansion and providing some level of confining stress. These two features: raising the sample, and the cooling water jacket, increase the thermal gradient and thermal shock at the top surface of the rock sample. The reported time of a comminution experiment begins once the rock sample of Barre Granite has been fully raised into the impinging supercritical water jet.

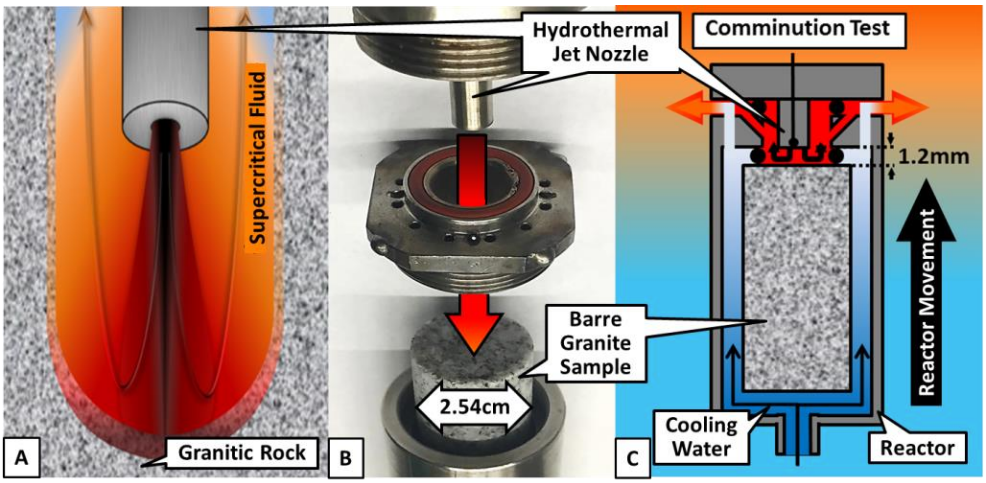

Figure 2: A) A sufficiently high temperature fluid impinging on a granitic rock surface induces a large thermal gradient in the rock resulting in rock removal by spallation (drilling). B) Experimental apparatus arrangement of 2.54cm diameter Barre Granite rock sample. C) The reactor chamber containing the rock sample and cooling water can be moved vertically upwards into the hydrothermal jet to increase thermal shock of the impinging fluid. The movement of the reactor chamber is bi-directional along the centerline allowing the rock sample to retract from the hydrothermal jet, halting the experiment at a select time interval.

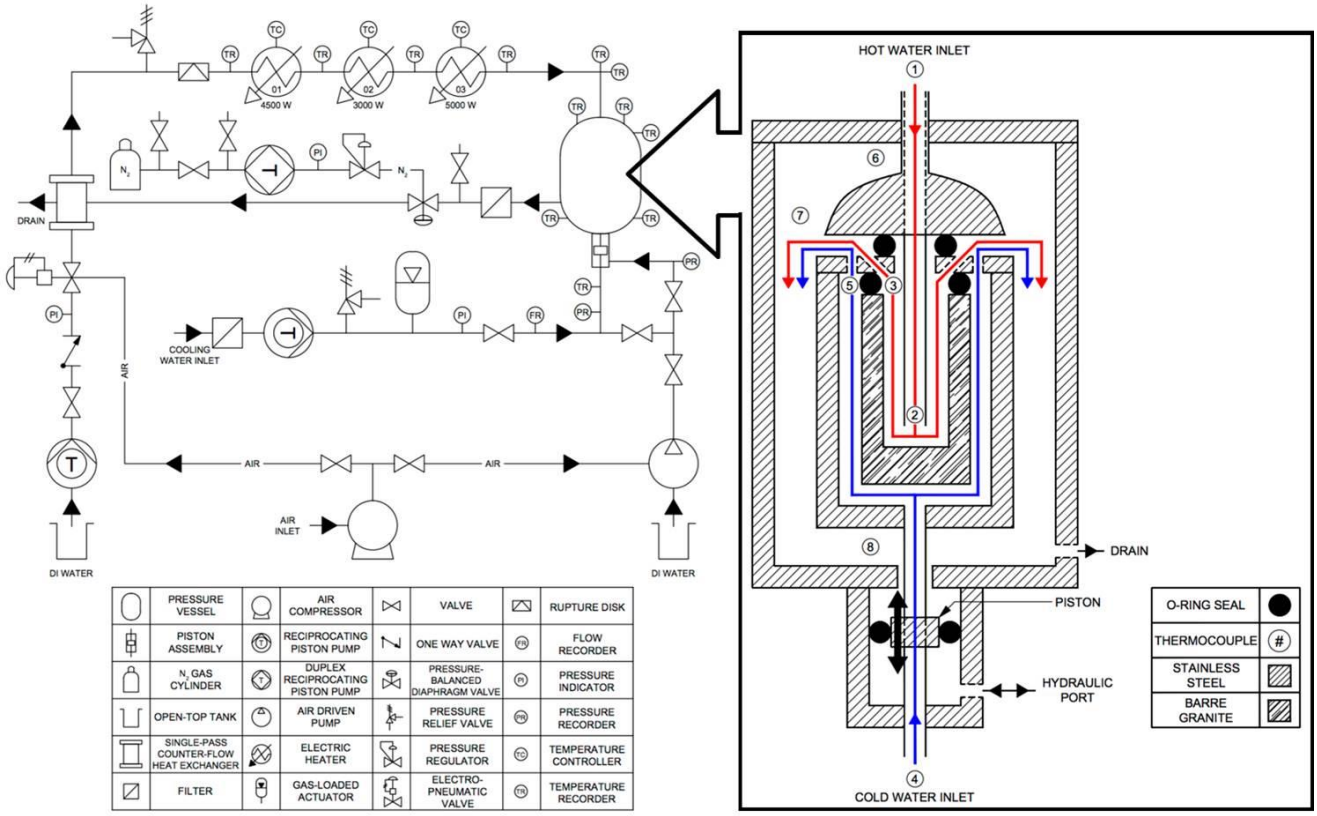

Figure 3: System piping and instrumentation diagram.

Three types of electrically heated hydrothermal jet experiments were performed: spallation, surface temperature, and heat flux, each had different testing configurations. The sources of uncertainty in the experimental results were identified as functions of system instrumentation, and fluid state properties. Using the Moffat method (Moffat, 1985), the combined error associated with the temperature, pressure, and flow rate sensors, including the fluid state properties were calculated to be less than 1.6%. Estimated errors are shown in Figure 4 as a function of fluid temperature within the temperature range studied.

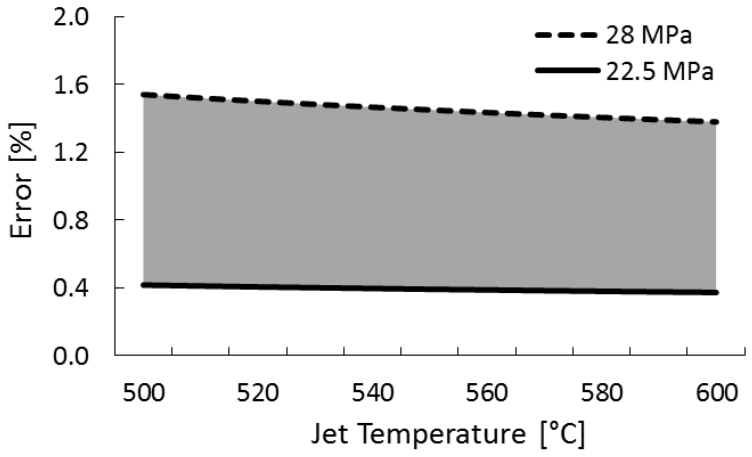

Figure 4: Estimated uncertainty in experimental data based on jet temperature.

3. COMMINUTION TEST RESULTS

Fifteen comminution tests at differing temperatures and pressures were performed, see Figure 5. The amount of damage to the samples' impinged surface corresponded in a non-linear fashion to the residence time in the reactor.

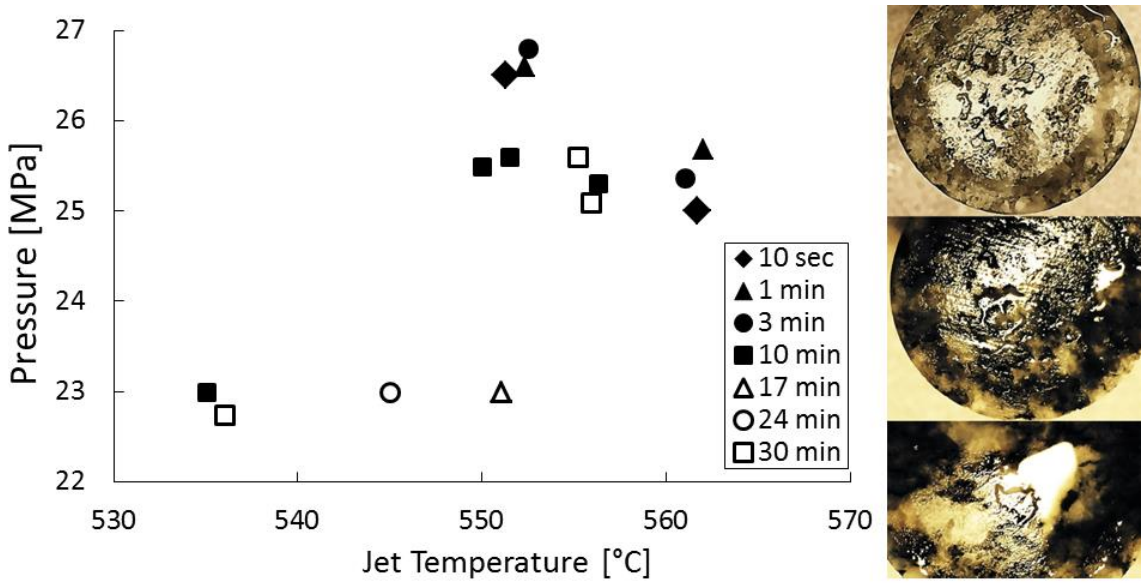

Figure 5: Spallation experiments conducted at a variety of pressures, temperatures, and time durations. Hydrothermal spallation test samples showing damage to the top surface.

The experimental results of the comminution tests were quantified by scanning a sample's top surface prior to the experiments with the Scanning Electron Microscope (SEM) to determine crystal/mineral composition, and after the experiments with a Laser-scanning Confocal Microscope (LSCM) which acted as a profilometer measuring the amount of mineral removed. The comminution tests consistently resulted in heterogeneous removal of surface material. Comparing the diminished areas to the SEM mineral map it was determined that exposing Barre Granite to a supercritical water jet preferentially removes quartz crystals, see Figure 6. Additionally, the boundaries of the subducted quartz grains are very distinct which further strengthens the argument for preferential removal of silica; however, no rock spalls were recovered from these experiments.

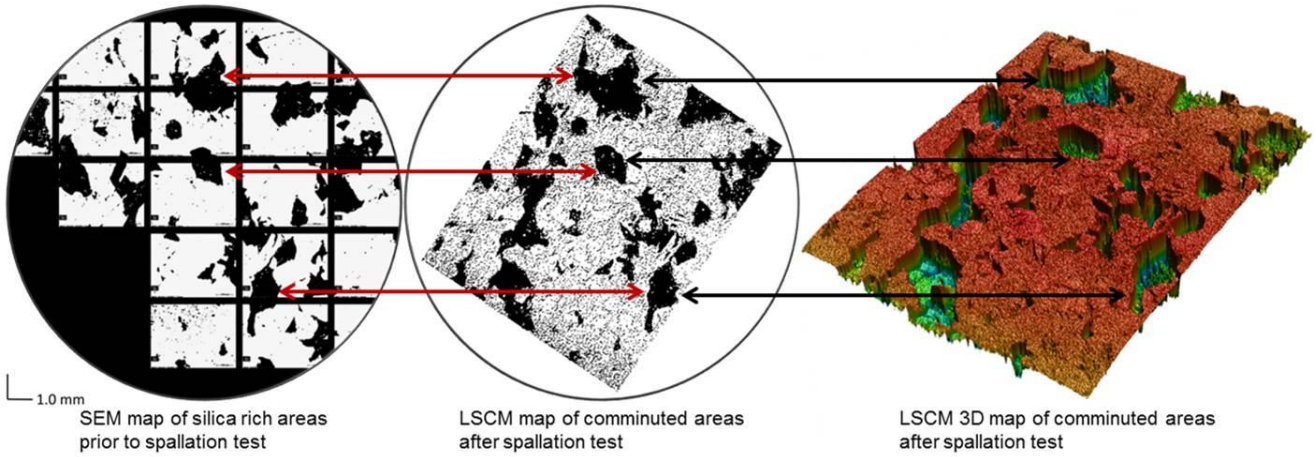

Figure 6: SEM images with color correction to highlight the silica rich quartz zones, compared against the LSCM map of the comminuted sample. The 'black' quartz crystals in the SEM image and the black subducted areas in the LSCM image correspond to each other. Observation indicates that quartz is preferentially removed. The z axis of the orthogonal view has a 10:1:1 scale with the x and y axis to accentuate the comminution effect.

The average composition of Barre Granite sample is 27.2% quartz, 19.4% potassium feldspar, 35.2% sodium feldspar, and 15.4% mica, with other minerals comprising the balance (Chayes, 1950); see Table 1. Preferential removal of quartz can be partially attributed to the difference in the coefficient of volumetric thermal expansion of quartz (4.98 [10^{-5}/°C]) and feldspar (~2 [10^{-5}/°C]), a greater than 2:1 ratio between these principal components (Robertson, 1988). The higher thermal expansion coefficient of quartz indicates that

significantly higher thermal stresses will be induced into the quartz crystals than the other surrounding minerals; however, other mechanisms for removing quartz must be considered before inferring that spallation has occurred. Note that since the impinging jet temperature was below 573°C, the α-β quartz phase transition should not play a role in its preferential removal.

Mineral	Formula	Composition Range	Composition Mean	Volumetric Thermal Expansion*	Thermal Conductivity**
		%	%	10^{-5}/°C	W/mK
Quartz	SiO_2	24.3 - 32.7	27.2	4.98	4 - 6.3
Microcline (K-feldspar)	$KAlSi_3O_8$	12.5 - 24.8	19.4	1.79	1.6 - 2.4
Plagioclase, (Albite)	$NaAlSi_3O_8$	30.3 - 40.4	35.2	2.24	1.7 - 2.3
Biotite	$K(Mg,Fe)_{2-3}Al_{1-2}Si_{2-3}O_{10}(OH,F)_2$	0.2 - 16.0	8.1	-	-
Muscovite	$KAl_2(Si_3AlO_{10})(OH)_2$	4.5 - 11.2	7.3	-	-
Other	CO_3^{2-} etc.	0.5 - 4.2	1.8	-	-

* averaged over the 20-400°C range, ** at 500°C

Table 1: Properties of Barre Granite (Chayes, 1950) (Robertson, 1988).

Flow stress or erosion, by the impact of the supercritical water on the sample's surface, were not found to be contributing factors to comminution. The Reynolds number associated with the hydrothermal jet in this temperature range was 48,000-60,000. At the experimental conditions, the maximum velocity associated with the supercritical jet was only 9 m/s, with a fluid density of about 70 kg/m^3, and a dynamic pressure difference between the jet nozzle and the rock surface less than 2 kPa, see Figure 7. The impinging pressure difference is about 5 orders of magnitude less than the pressure used to cut Barre Granite with a high velocity water jet (Summers, 1972). Additionally, the acute edges along quartz boundary lines show no signs of erosion.

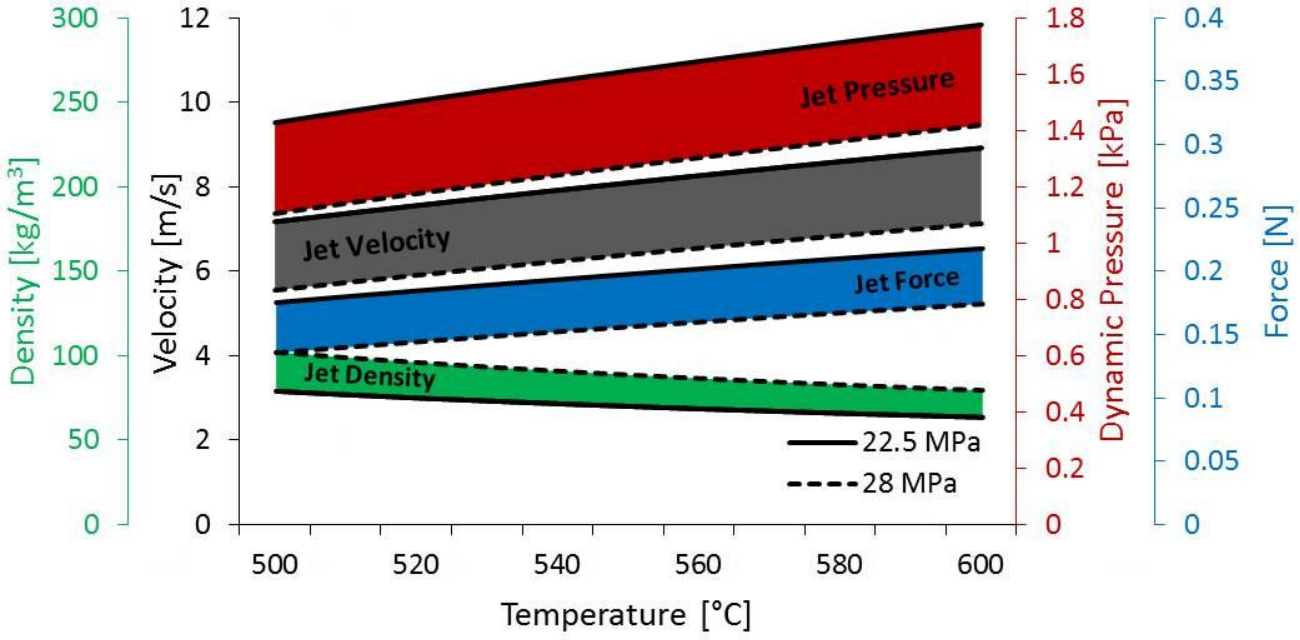

Figure 7: The range of jet nozzle velocity, and pressure difference between the jet nozzle and rock surface.

Another mechanism which may remove quartz from the rock surface is dissolution. The reversible chemical reaction for the dissolution of quartz in pure water is $SiO_{2(s)} + 2H_2O_{(aq)} \Leftrightarrow H_4SiO_{4(aq)}$. Where the forward dissolution reaction rate (Rimstidt & Barnes, 1980) (Worley, 1994):

$$r_{forward} = k_{forward} \frac{A_{surface}}{M_{water}} \left[\frac{mol}{kg \times s} \right] \tag{1}$$

incorporates an active effective surface area, $A_{surface}$, the mass of water in the system, M_{water}, and the dissolution rate constant, $k_{forward}$. The empirical equation for $k_{forward}$ of quartz in pure water, based on the nominal geometric surface area based on the analysis of (Worley, 1994) is given by:

$$k_{forward} = (276 \pm 193) \exp\left[\frac{(90.1 \pm 2.5)}{RT} \right] \left[\frac{mol}{m^2 \times s} \right] \tag{2}$$

The parameters with 95% confidence levels in Equation 2 were fitted by linear regression to the data shown in Figure 8. This dissolution rate constant can be used to compare the removal of quartz from the comminution experiments to estimate how much quartz would be removed by dissolution alone. Calculating the dissolution rate constant for the comminution experiments was achieved by dividing silica's density, ρ_{solute}, by its molar mass, M_{solute}, then multiplying by the depth of the subducted area, Z, and finally dividing by the duration of the experiment, t, $k_{forward} = \frac{\rho_{solute} Z}{M_{solute} t} \left[\frac{mol}{m^2 \times s} \right]$. For all tests conducted in this study $k_{forward}$ values were greater by an order of magnitude or more than indicated by Equation 2. The difference in the observed comminution rate from the quartz dissolution rate implies that a secondary mechanism preferentially removing quartz exists.

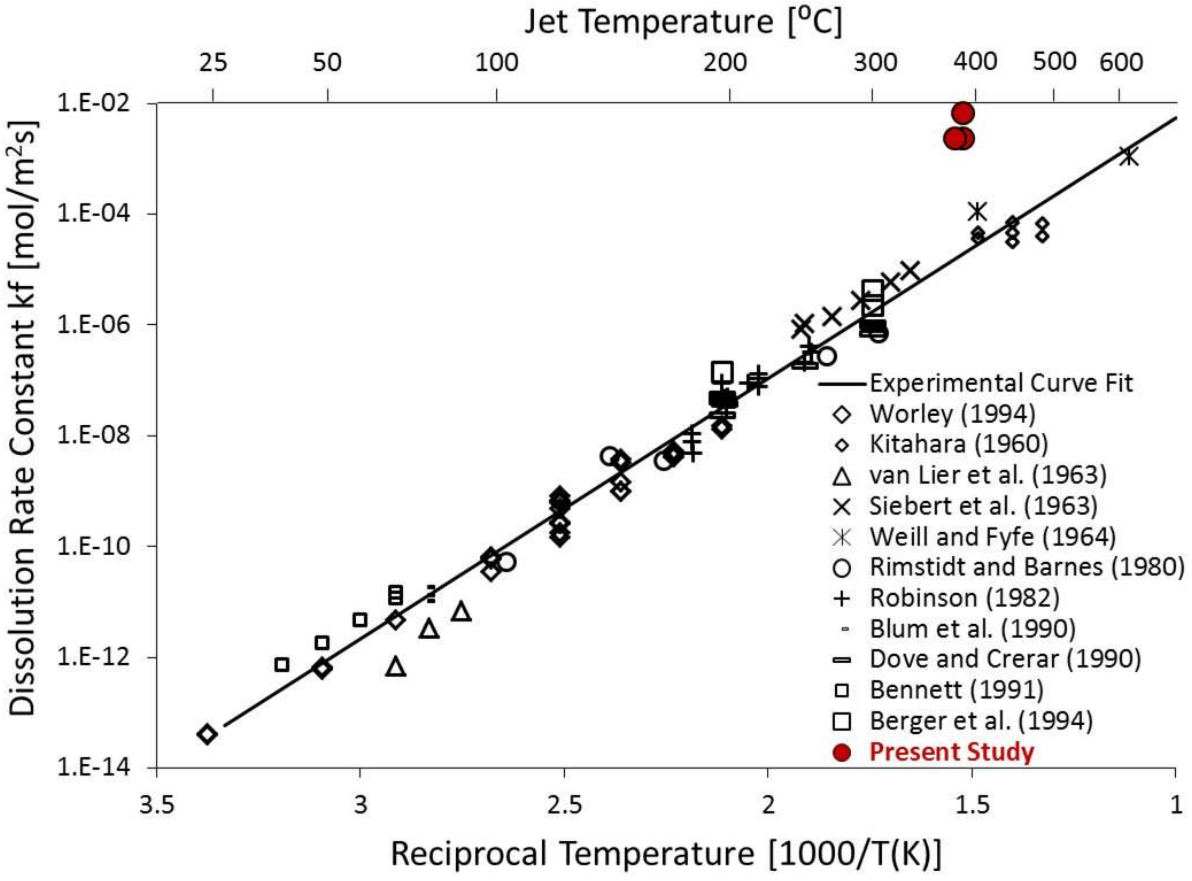

Figure 8: Arrenhius plot of quartz dissolution data including this study's comminution experiments (Worley, 1994).

Further support of this interpretation comes via visual analysis of the experiment samples, which indicates that the comminution rate was higher during the first 10 to 17 minutes of the experiment (once the rock sample has been raised into the jet) then tapers off in the in the latter period of the experiment as more of the exposed quartz is removed. However, quantification of this phenomena poses experimental challenges due to the heterogeneity of the mineral composition and grain structure of Barre Granite.

Clearly another mechanism other than rapid erosion and dissolution is controlling the removal of quartz. One hypothesis is that spallation is in fact occurring strictly within the quartz grains, but in a much more localized fashion than observed in previous open air flame jet experiments. There are several possible reasons why more localized spallation is occurring under hydrothermal conditions:

1) The conditions achieved at the rock surface may truly be approaching the lower limit temperature and/or heat flux limit for which spallation can occur, and thus it is only in the quartz grains (with a higher coefficient of thermal expansion and higher thermal conductivity) where the induced thermal stresses are sufficient to prompt intra-grain fracture growth. Inter-granularly, the lower thermal conductivity in the non-quartzite minerals will partially insulate against the heat transfer along quartz grain boundaries, preferentially increasing the thermal stresses in the quartz grains.

2) Engineering analysis of conventional rotary drilling suggests that higher hydrostatic pressures hinder drilling rates because the comminuted material cannot be removed from the rock surface as easily. This effect may be present to some degree in hydrothermal spallation as well, where, to form a spall, cracks must propagate in the plane parallel to the impinged surface, but the high hydrostatic pressure is acting to prevent crack growth along that plane.

3) The hydrostatic pressure effectively generates a tensile stress parallel to the rock surface due to Poisson effect (Hibbler, 2016), thereby counteracting the compressive stress in this plane caused by thermal expansion which promotes spallation. The cylindrical rock sample used in these experiments has a hydrostatic pressure applied on all sides, but the compressive stress in the radial direction may diminish towards the center of the impinged top surface such that the local tensile stress component caused by the hydrostatic pressure in the axial direction is dominant.

4) Insufficient confining radial and axial stresses may be inhibiting continuous spallation. Successful hydrothermal spallation was achieved by Potter Drilling with applied radial and axial stresses two and three times the confining hydrostatic pressure and their rock samples had diameters four times the diameters of cores used in this study (Potter Drilling, 2008).

4. SURFACE TEMPERATURE MEASUREMENTS

Quantifying the surface temperature of the rock sample is essential to predict spallation (Wilkinson, 1993). To measure the surface temperature a rock sample was cored from the underside until only a very thin layer of rock, 0.65mm, remained at the top surface, see Figure 9. The ratio of diameter of the cored out section to top cap thickness was 10:1 allowing the assumption of horizontal isotherms, and vertical heat flow at the centerpoint. A 1/16" (1.6 mm) thermocouple stripped of its shielding (mitigating conduction losses) was placed in contact with the underside of the thin top cap, the remaining chamber volume was filled with thermal conductive paste and sealed. The contact resistance of the thermocouple and thermal resistivity of the granite was not included in the surface temperature analysis because of the minimal thickness of the top cap, and the short 1.8 mm distance between the jet and surface temperature thermocouples. Each of the surface temperature measurements were averaged over a greater than 30 second "steady state" period during which the temperature did not fluctuate by more than one degree.

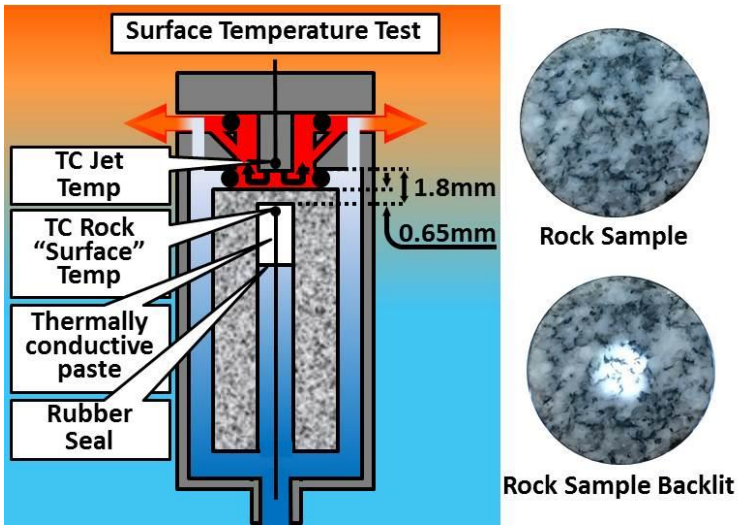

Figure 9: The distance between the two thermocouples measuring jet and surface temperature was 1.8mm. Backlighting the rock sample shows the transparency of the 0.65 mm thick granite "cap".

The measurements indicated that the surface temperature of the granite rock sample undergoing comminution was lower than the impinging supercritical water jet. And the difference in temperature between the surface of the rock and hot water jet increased as the temperature of the jet increased, as shown in Figure 10. Both the decreasing fluid density and increasing Reynolds number of the impinging jet show why heat transfer to the rock surface will be strongly affected by the increasing jet temperature, Figure 10.

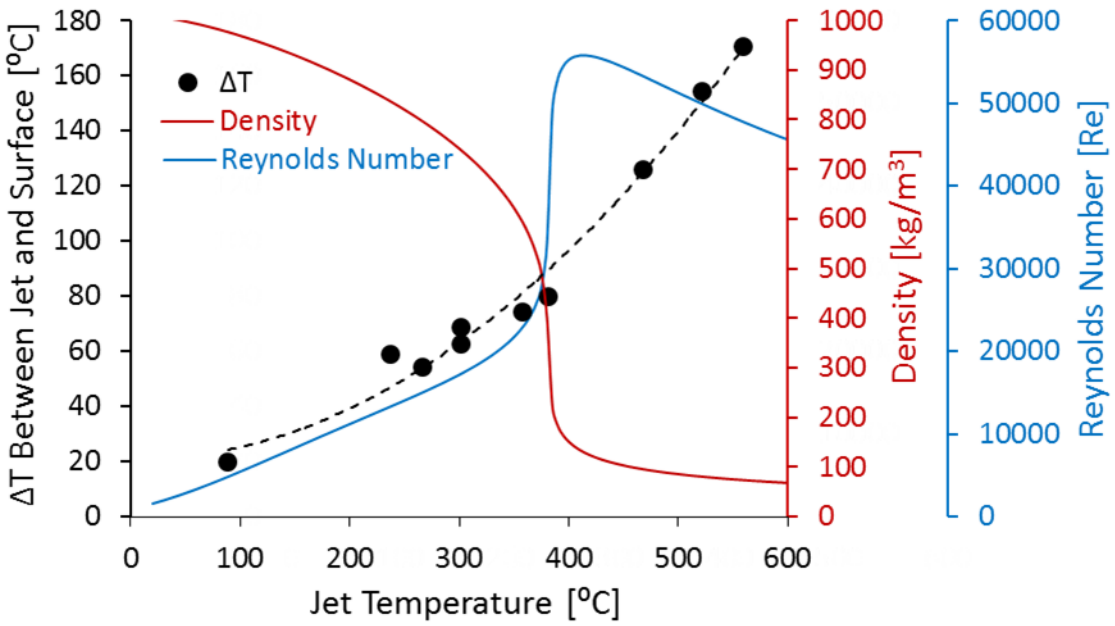

Figure 10: Estimated temperature difference, ΔT, between the surface of the rock and the hydrothermal jet as a function of the hydrothermal jet temperature at 24 MPa. The data points represent steady state temperature measurements, the trendline is a best fit regression approximation.

5. HEAT FLUX MEASUREMENTS

A measured heat flux through the rock surface is the second essential component in determining the likelihood of rock spallation. The experiments performed were based on the energy balance $\dot{q}_{heatflux} = \dot{q}_{in} - \dot{q}_{exitingH_2O} = \frac{\dot{m}\Delta H}{A}$ where $\dot{q}$ has units of $\frac{W}{m^2}$. $\dot{m}$, ΔH, and A are mass flow rate, enthalpy and area respectively. As such a standard rock sample was cored from the top to create a cylindrical chamber with side walls and base of equal thickness. The area hollowed out is the downward projection of the top area exposed to the hydrothermal jet in comminution tests, providing an approximation of the experimental conditions. Two thermocouples were placed at equal height, one within the incoming jet the other in the exit water. The height positioning of both thermocouples was determined by a 1:5 ratio of the annular width (between the incoming jet stem and sample's side wall) to the top edge of the rock sample, mitigating the edge effects of increased heat loss from the top metal portion of the reactor, Figure 11. The confining pressure and temperature difference between the two thermocouples was used to calculate the change in enthalpy, ΔH, of pure water using thermodynamic properties for pure water from NIST. (NIST REFPROP, 2013). System cooling water flow rates were varied from the experimental standard of 2.8 LPM to see the impact they had on heat flux; the lower flow rate experiments of 1.8 LPM were cut short due to the pressure vessel exceeding maximum temperature of 80°C.

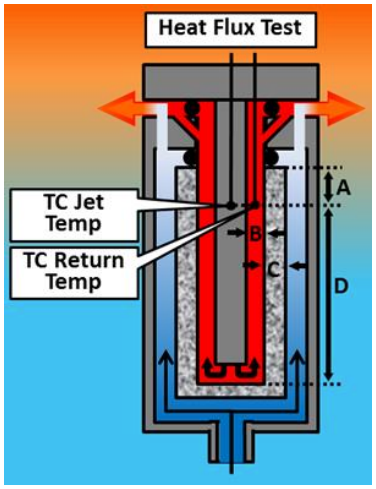

Figure 11: Experimental configuration for the heat flux tests. To mitigate edge effects the ratio of A:B was 5:1, D:A 5:1, C:D 19:1.

Correlating the experimental heat flux data to the experimentally determined rock surface temperature indicates that heat flux through the rock increases up to a point and then drops off rapidly, Figure 12. This experimental result is consistent with water's combined thermodynamic properties of density and specific heat, volumetric specific heat [W/m^{3}K], as seen in Figure 12. The change in volumetric specific heat varies the energy available for transfer in the fluid while the density limits the transfer of that heat to the rock. The differences in the slope of the heat flux lines correspond to different cooling water flow rates that jacket the exterior of the rock sample. As the cooling water flow rate increases it extracts more energy, increasing the heat flux. Additionally heat conduction through the rock, $\dot{Q} = -kA\frac{dT}{dx}$, is limited by the rock thermal conductivity, k. As shown in Figure 12, k for Barre Granite is inversely related to temperature (Hueze, 1983), thus lowering the heat flux linearly as the temperature increases for the same imposed temperature gradient.

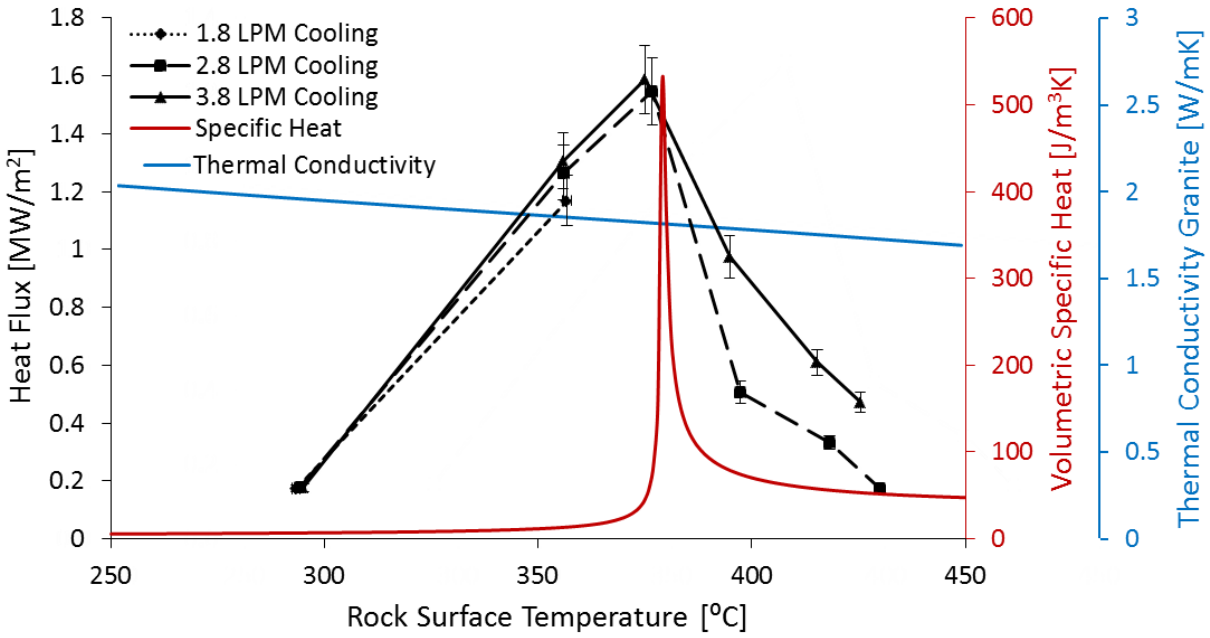

Figure 12: Heat flux as a function of experimentally determined rock surface temperature. The ratios of supercritical jet flow to the cooling water flow rates of 1.8, 2.8 and 3.8 liters per minute, LPM, were 1:7.5, 1:11.5, 1:15.8, respectively. The volumetric specific heat of water, and thermal conductivity of granite at a pressure at 24 MPa were calculated using the experimentally determined rock surface temperature.

The experimentally determined hydrothermal spallation heat flux data was compared to previous work in flame jet and laser spallation on Barre Granite (Rauenzahn, 1986) (Wilkinson, 1989). See Figure 13. All of the experimental data from this study were below the temperature of previous thermal spallation experiments The heat fluxes were also near or below the lowest values measured for flame or laser induced spallation. Therefore, while the relationship between surface temperature and heat flux is not fully understood there appears to be a threshold temperature/heat flux that must be reached to induce true thermal spallation. Potter Drilling identified the onset of hydrothermal spallation at a water jet temperature of 700°C (Potter Drilling, 2008). Linearly extrapolating the prediction of rock surface temperature from this study's water jet temperature data indicates a minimum surface temperature of 500°C for Potter Drilling. This is still 80°C higher than the maximum capability of the hydrothermal spallation drilling apparatus at Cornell. Therefore, continuous hydrothermal spallation could not be achieved at the temperatures and heat fluxes capable of being studied with the existing equipment.

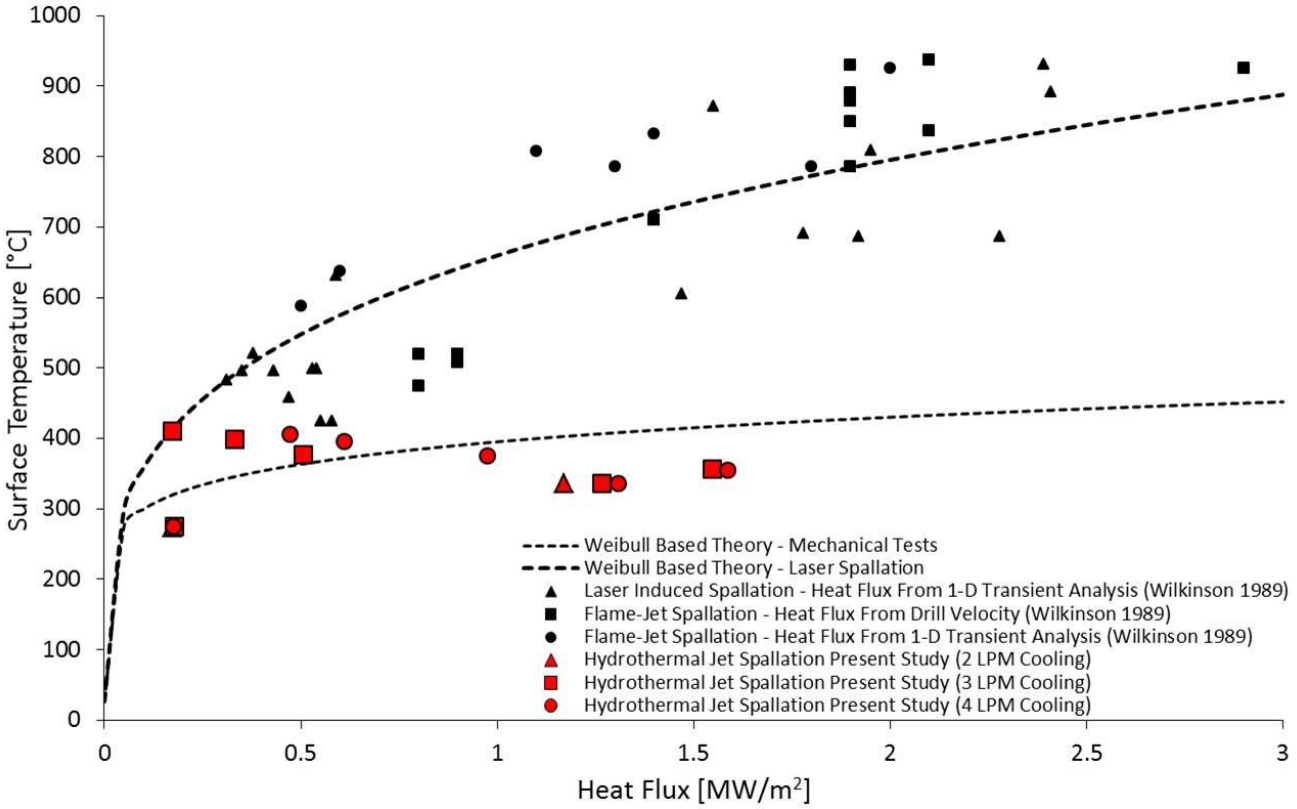

Figure 13: Experimentally determined heat flux and surface temperature for hydrothermal jet spallation compared to flame jet and laser spallation. This study's hydrothermal experiments were conducted at surface temperatures below previous experimentally determined thresholds for gas immersed spallation.

6. CHEMICAL ENHANCED SPALLATION

Chemically enhanced hydrothermal spallation is the addition of chemicals into the impinging supercritical water jet stream to weaken the constituent minerals. In principle, this could result in increased rates of rock removal to promote spallation at higher rates and lower jet temperatures. In 2004, Richard S. Polizzotti received a patent for chemically enhanced spallation drilling (Polizzotti, 2004) using sodium hydroxide, NaOH. The preferred jet temperatures quoted in the patent ranged from 800-1200°C with concentrations greater than 0.025 mol NaOH/kg H_2O. However, the data were not made publicly available, nor were the claims independently verified. Therefore, this part of the investigation focused on evaluating chemically enhanced spallation under well-defined conditions to quantitatively measure and model the effect of jet temperature and NaOH concentration on rock removal rates.

Over jet temperatures from 550°C to 570°C and NaOH concentrations from 0.15 to 2.69 % w/w Barre Granite was removed at appreciable rates as seen in Figure 14. Circular holes were produced into the rock of approximately equal diameter to the round surface area exposed to the NaOH hydrothermal jet. The depth drilled was dependant on the molality of NaOH, Figure 15. However, since the water jet drilling nozzle and rock sample were stationary during the test only a portion of the rock sample was penetrated. The same experimental conditions as pure water hydrothermal spallation tests was maintained except that all tests were run for 10 minutes.

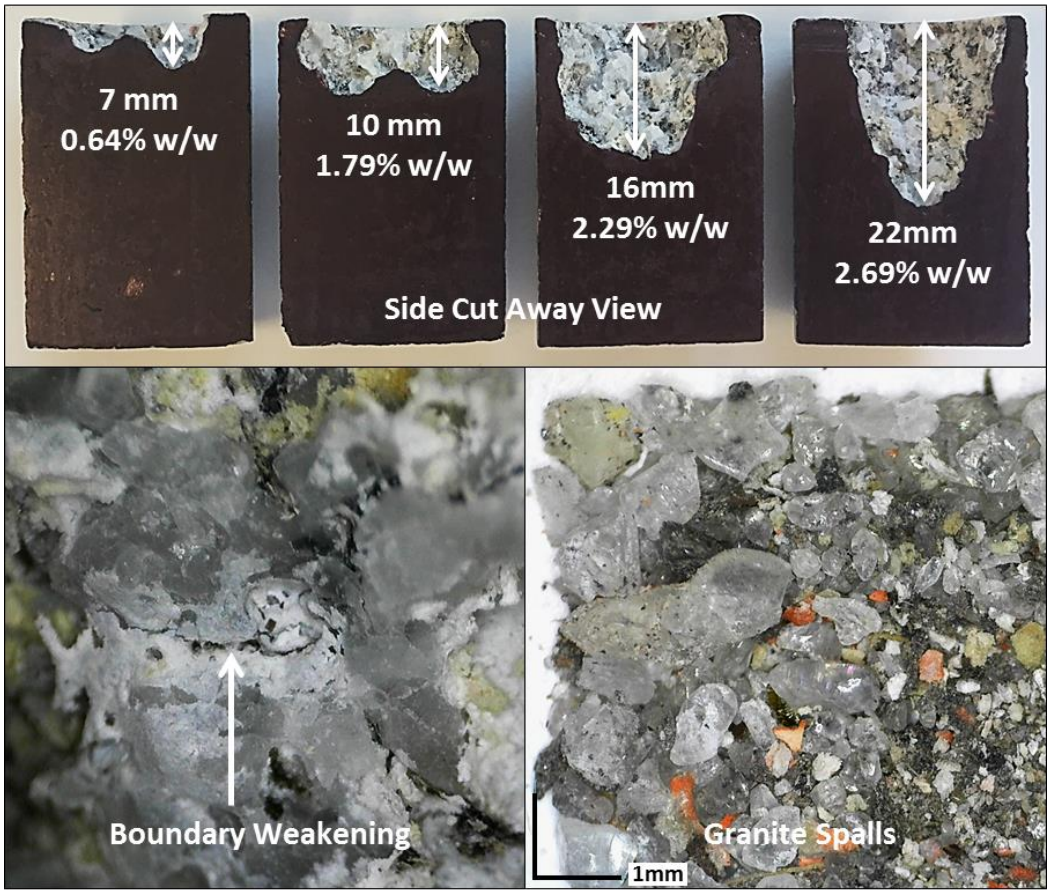

Figure 14: Chemical enhanced hydrothermal spallation results. Top: Side cut Barre Granite samples show significant dissolution and spallation. These experiments used 0.64-2.69% w/w NaOH, at 25 MPa, 380-420°C, for 10 minutes. Bottom left: Preferential weakening along crystal boundaries due to the absence of feldspar. Bottom right: Predominantly pebble shaped quartz spalls ranging in size (red color is O-ring staining).

Chemical dissolution was a significant factor in granite removal because the spalls recovered were not similarly sized disk shaped flakes traditionally recovered from thermal flame spallation, but rather of various sizes and rounded like small pebbles. In addition, the mass of spalls collected were only a fraction of the total mass removed, and a significant amount of very fine powder and precipitate were recovered from the back-pressure valve. Clearly, increased solubility of silica at high pH is occurring but quantification was not possible as no measurements were made of concentration in the diluted effluent water in these experiments. The captured spalls were primarily quartz, implying a more rapid comminution of feldspar by a combination of possible mechanisms like dissolution and geochemical alteration. This was consistent with the post spallation images that indicated preferential boundary weakening around quartz crystals. The depth of the cavity and absolute mass of granite removed appears to corresponded to increased solvent molality, but further experiments will be required to verify this phenomena, Figure 15. The relative mass of granite removed by a given mass of NaOH appears to stabilize after the onset of spallation despite the increased distance between the dissolving rock face and the jet nozzle increasing fluid mixing, thereby reducing the amount of unsaturated fluid reaching the spallation front, and reducing solvent temperature.

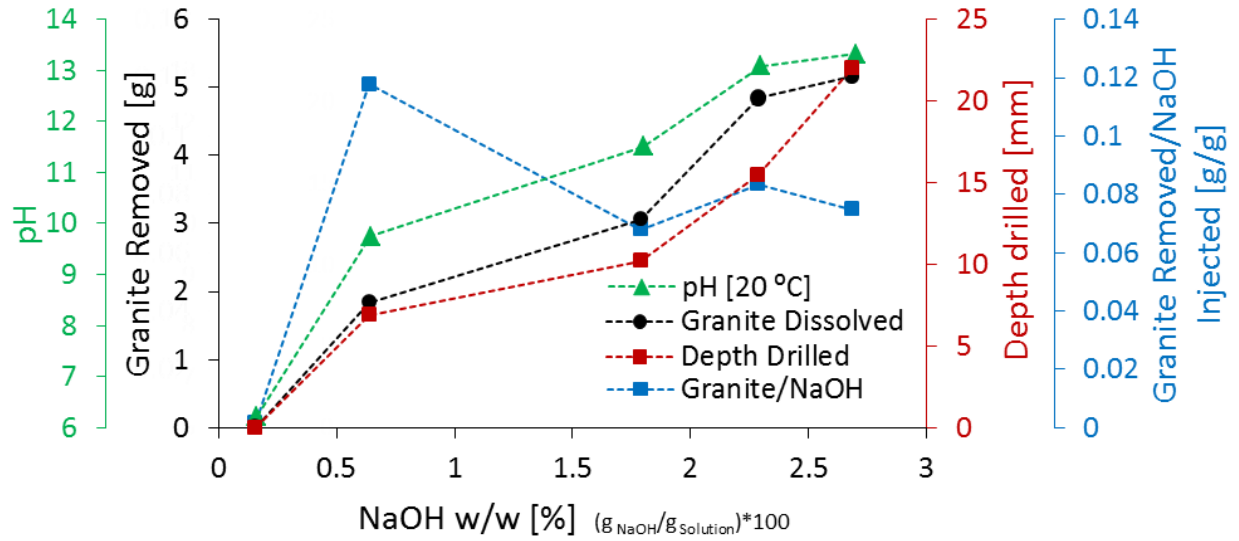

Figure 15: The mass of granite removed and the depth drilled increases with increasing NaOH molality. Once spallation is initiated the ratio of granite removed to NaOH injected stabilizes with increasing solvent molality. All experiments ran for 10 minutes.

Modelling possible drilling rates based on the experimental data relied on the assumptions that granite dissolution/erosion/spallation is similar in process to that of quartz dissolution. This is proposed because quartz is a significant component of Barre Granite and feldspar contains silicates as well. Another assumption is that the analysis of possible comminution mechanisms for granite using pure supercritical water apply in this case, eliminating erosion and focusing on the chemical enhancement. Regression analysis that accounts for the influence of temperature and NaOH concentrations is sufficient to quantify the experimental data.

The net reaction rate of dissolution, r_{net}, is a subtraction of the reverse reaction rate, $r_{reverse}$, (re-deposition of dissolved minerals) from $r_{forward}$, Equation 1. However, $r_{forward}$ dominates since the injected solvent was not close to saturation, therefore $r_{reverse}$ can be neglected from the analysis (Worley, 1994).

$$r_{net} = \frac{dm_{granite}}{dt} = r_{forward} - r_{reverse} \approx r_{forward} \left[\frac{mol}{kg \times s} \right] \tag{3}$$

Multiplying Equation 3 though by molar mass of NaOH

$$r'_{net} = \frac{d\left(\frac{M_{granite}}{M_{solvent}} \right)}{dt} = r'_{forward} = k_{forward} \frac{A_{surface}}{M_{solvent}} \left[\frac{kg_{solute}}{kg_{solvent} \times s} \right] \tag{4}$$

$M_{granite}$ [kg] is the mass of granite removed, $M_{solvent}$ [kg] is the mass of injected solvent which is water with a NaOH concentration, and $k_{forward}$ is dissolution rate constant with adjusted units of [$kg_{solute}/(m^2 s)$]. The effective surface area term, $A_{surface}$ is no longer constant for spallation due to increased rock removal over time. Using the assumption of cylindrical spallation with a hemispherical front as the jet moves into the rock the change in nominal surface area exposed to the chemical jet becomes a function of depth, which is a function of time. The surface area equation $A_{surface} = \frac{\pi D^2}{2} + \pi D h(t)$ can be rewritten as $A_{surface} \approx \frac{\pi D^2}{2}$ because the primary rock face being eroded has a constant hemispherical area advancing in the z-direction. Also, once the solvent has interacted with the hemispherical spallation front (base of the cylinder) the remaining chemical reactions with the sidewalls, $\pi D h(t)$, are of less consequence and of lower magnitude since the solvent has lowered in temperature and contains some solute. Using this hemispherical area assumption the right hand side of Equation 4 becomes

$$r'_{net} = k_{forward} \frac{\frac{\pi D^2}{2}}{M_{solvent}} \left[\frac{kg_{solute}}{kg_{solvent} \times s} \right] \tag{5}$$

Extending the same hemispherical spallation front assumption to the granite rock face area, $A_{granite}$, in the left-hand side of Equation 4.

$$r'_{net} = \frac{d\left(\frac{M_{granite}}{M_{solvent}}\right)}{dt} = \left(\frac{1}{M_{solvent}}\right)\frac{dV_{granite}\,\rho_{granite}}{dt} = \left(\frac{A_{granite}\,\rho_{granite}}{M_{solvent}}\right)\frac{dz}{dt} = \left(\frac{\frac{\pi D^2}{2}\rho_{granite}}{M_{solvent}}\right)\frac{dz}{dt}\left[\frac{kg_{solute}}{kg_{solvent}\times s}\right] \tag{6}$$

Combining Equations 5 and 6 allows for the cancellation of the surface area terms providing an effective "drilling rate", $\frac{dz}{dt}$

$$\frac{dz}{dt} = \frac{k_{forward}}{\rho_{granite}}\left[\frac{m}{s}\right] \tag{7}$$

$\rho_{granite}$ is the density of granite. Based on Worley's (1994) work, $k_{forward}$ can be expressed as

$$k_{forward} = k(T)_{OH^-,Na^+}\, m_{OH^-}^{b}\, m_{Na^+}^{c}\left[\frac{kg}{m^2\times s}\right] \tag{8}$$

Where $k(T)_{OH^-,Na^+}$ is a temperature dependent constant, and $m_{OH^-}^{b}$ and $m_{Na^+}^{c}$ are the molality's of the hydroxide and sodium ions. Equation 7 shows that $\frac{dz}{dt}$ will depend directly on $k_{forward}$, which Equation 8 states is a function of temperature, NaOH concentration and pH. Therefore, subsequent study will continue to investigate and model temperature/molality effects on chemically enhanced comminution.

7. CONCLUSION AND FUTURE DIRECTIONS

Spallation experiments were performed on Barre Granite using pure supercritical water at 535-565°C at 22.5-27 MPa. This temperature range was selected to examine the low temperature limit required to induce hydrothermal jet spallation, while the high water pressures used simulate a deep, water filled wellbore. The main goal of the experiments was to achieve hydrothermal spallation of the rock samples' surface, to develop an experimental basis upon which further analyses can be conducted.

The pure water experiments demonstrated the preferential comminution of the quartz grains. This could indicate the onset of hydrothermal jet spallation even though no rock spalls were directly collected, because the removal of the quartz was greater than can be explained by erosion and silica dissolution alone. Suggesting, at the very least, that hydrothermal spallation was a secondary mechanism for preferential quartz comminution.

The temperature difference between the experimental rock surface and the impinging water jet increased with increasing water temperature, decreasing the effective heat transfer rate to the rock surface. Heat flux to the rock surface was measured and found to correlate to the volumetric specific heat of water. All spallation measured surface temperatures and heat fluxes from these hydrothermal spallation experiments in pure water were lower than those observed for flame jet and laser heating. In a separate set of experiments to evaluate the potential of chemically enhancing spallation, NaOH was injected into the supercritical jet to increase pH. This led to significantly increased rates of granite rock removal in comparison to the pure water jets at the same temperatures and pressures. The penetration depth appears to correspond linearly to NaOH molality which varied from 0.15 to 2.69 % w/w. Accelerated dissolution induced by NaOH was observed because the quartz spalls recovered had predominately rounded surfaces rather than disk shaped flakes, and the feldspars appeared to comminute more rapidly thereby weakening inter-grain boundaries.

Future work will focus on completing the chemically enhanced dissolution experiments at different temperatures and concentrations to enable the prediction of an effective drilling rate based on jet temperature and molality.

8. ACKNOWLEDGEMENTS

These experimental results would not have been possible without the initial creative work of Bob Potter on spallation drilling. The authors are also grateful to Jared Potter for his interest in this research and for donating a high-pressure experimental apparatus. Many thanks go to Chad Augustine for his initial work at MIT that experimentally demonstrated that hydrothermal flames could be produced in supercritical water and used to spall rock, and to Rick M. Rauenzahn and Mark Wilkinson for their pioneering efforts in characterizing and modeling flame jet and laser induced spallation and finally to W. Gabe Worley for his work on quartz dissolution kinetics in hydrothermal NaOH solutions. The partial support of this work by the Cornell Energy Institute and the Department of Chemical and Biomolecular Engineering is also gratefully acknowledged.

REFERENCES

Augustine, C. R.: Hydrothermal Spallation Drilling and Advanced Energy Conversion Technologies for Engineered Geothermal Systems. Doctoral Thesis. Massachusetts: Massachusetts Institute of Technology, (2009).

Augustine, C. R. & Tester, J. W.: Hydrothermal flames: From phenomenological experimental demonstrations to quantitative understanding. The Journal of Supercritical Fluids, Volume 47, (2009), p. 415–430.

Benett, P. C.: Quartz dissolution in organic-rich aqueous systems. Geochimica et Cosmochimica Acta, Volume 55, (1991), pp. 1781-1797.

Berger, G., Cadore, E., Schott, J. & Dove, P. M.: Dissolution rate of quartz in lead and sodium electrolyte solutions between 25 and 300°C: Effect of the nature of surface complexes and reaction affinity. Geochimica et Cosmochimica Acta, 58(2), (1991), pp. 541-551.

Blackwell, D. et al.: Temperature-At-Depth Maps For the Conterminous U.S. and Geothermal Resource Estimates. s.l., Geothermal Resource Council, Vol 35, (2011), (GRC 1029452).

Blum, A. E., Yund, A. R. & Lasaga, A. C.: The effect of dislocation density on the dissolution rate of quartz. Geochimica et Cosmochimica Acta, Volume 54, (2011), pp. 283-297.

Browning, J.: Flame-Jet Drilling in Conway, N.H. Granite, Work Order #4-L10-2889R-1: University of California, (1981).

Chayes, F.: On a distinction between late-magmatic and post-magmatic replacement reactions, Montpelier: Vermont Agency of Natural Resources, (1950).

Dove, P. M. & Crerar, D. A.: Kinetics of quartz dissolution in electrolyte solutions using a hydrothermal mixed flow reactor. Geochimica et Cosmochimica Acta, Volume 54, (1990), pp. 955-969.

Finger, J. & Blankenship, D.: Handbook of Best Drilling Practices for Geothermal Drilling, Albuquerque: Sandia National Laboratories, (2010).

Fox, D. B., Sutter, D. & Tester, J. W.: The thermal spectrum of low-temperature energy use in the United States. Energy and Enviromental Science, 4(10), (2011), pp. 3731-3740.

Hibbler, R. C.: Mechanics of Materials. 10, ISBN-13: 978-0134319650 ed. s.l.:Pearson, (2016).

Hillson, S. D. & Tester, J. W.: Heat Transfer Properties and Dissolution Behavior of Barre Granite as Applied to Hydrothermal Drilling with Chemical Enhancement. Stanford, CA, Fortieth Stanford Geothermal Workshop, Stanford University, (2015).

Hueze, F.: High-Temperature Mechanical, Physical and Thermal Properties of Granitic Rocks --A Review. International Journal of Rock Mechanics and Mining Sciences & Geomechanics Abstracts, 20(1), (1983), pp. 3-10.

Kithara, S.: The solubility equilibrium and the rate of solution of quarts in water at high temperatures and high pressures. The Review of Physical Chemistry of Japan, 30(2), (1960), pp. 122-130.

Macini, P. & Mesini, E.: Rock-Bit wear in ultra-hot holes. Delft, Proc. Int. Conf. "Eurock'94", (1994), pp. 223-230.

Moffat, R. J.: Using Uncertainty Analysis in the Planning of and Experiment. Journal of Fluids Engineering, June, Volume 107, (1985), pp. 173-178.

NIST REFPROP.: NIST Standard Reference Database 23, Version 9.1. s.l.:NIST for the U.S. Secretary of Commerce on the behalf of the United States of America (2013).

Polizzotti, R. S.: United States, Patent No. 6742603 B2, (2004).

Potter Drilling.: Stage I Report, Laboratory testing and modeling of hydrothermal spallation drilling, Redwood City: Potter Drilling, (2008).

Rauenzahn, R. M.: Analysis of Rock Mechanics and Gas Dynamics of Flame-Jet Thermal Spallation Drilling. Doctoral Thesis. Cambridge: Massachusetts Institute of Technology, (1986).

Rauenzahn, R. M. & Tester, J. W.: Flame Jet Induced Thermal Spallation as a Method of Rapid Drilling and Cavity Formation. Las Vegas, s.n., (1985).

Rauenzahn, R. M. & Tester, J. W.: Rock Failure Mechanisms of flame-jet thermal spallation drilling - theory and experimental testing. International Journal of Rock Mechanics and Mining Sciences & Geomechanics Abstracts, 26(No. 5), (1989), pp. 381-399.

Rimstidt, J. D. & Barnes, H. L.: The kinetics of silica-water reactions. Geochimica et Cosmochimica Acta, 44(11), (1980), pp. 1683-1699.

Robertson, E. C.: Thermal properties of rocks, Reston: United States Department Of The Interior Geological Survey, (1988).

Robinson, B. A.: Quartz Dissolution and Silica Deposition in Hot Dry Rock Geothermal Systems, M.S. Thesis. Cambridge: Massachusetts Institute of Technology, (1982).

Seibert, H., Youdelis, W. V., Leja, J. & Lilge, E. O.: The kinetics of the dissolution of crystalline quartz in water at high temperatures and pressures. Unit Processes in Hydrometallurgy, Volume 24, (1963), pp. 284-299.

Stathopoulos, P., Meier, T. & Rudolf von Rohr, P.: Hydrothermal flame impingement experiments. Combustion chamber design and impingement temperature profiles. The Journal of Supercritical Fluids, Volume 89, (2014), pp. 48-57.

Summers, D. A.: Water jet cutting related to jet and rock properties. University Park, Pennsylvania, s.n., (1972).

Tester, J. W. et. al.: The Future of Geothermal Energy: Impact of enhanced geothermal systems (EGS) on the United States in the 21st century, s.l.: Massachusetts Institute of Technology and Department of Energy Report, Idaho National Laboratory, INL/EXT-06-11746, (2006).

Ürge-Vorsatz, D. et al.:Heating and cooling energy trends and drivers in buildings. Renewable and Sustainable Energy Reviews, Volume 41, (2015), pp. 85-98.

VAN Lier, J. A., DE Bruyn, P. L. & Overbeek, J. T. G.: The solubility of quartz. The Journal of Physical Chemistry, Volume 64, (1960), pp. 1675-1682.

Weill, D. F. & Fyfe, W. S.: The solubility of quartz in H_2O in the range of 1000-4000 bars and 400-550°C. Geochimica et Cosmochimica Acta, Volume 28, (1964), pp. 1243-1255.

Wilkinson, M. A.: Computational Modelling of the Gas-Phase Transport phenomena and Experimental Investigation of Surface Temperatures During Flame-Jet Thermal Spallation Drilling. Doctoral Thesis. Cambridge: Massachusetts Institute of Technology, (1989).

Wilkinson, M. A. & Tester, J. W.: Experimental measurement of surface temperatures during flame-jet induced thermal spallation. Rock Mechanics and Rock Engineering, 26(1), (1993), pp. 29-62.

Wilkinson, M. A. & Tester, J. W.: Experimental Measurement of Surface Temperatures During Flame-Jet Induced Thermal Spallation. Rock Mechanics and Rock Engineering, 26(1), (1993), pp. 29-62.

Williams, R. E.: The thermal spallation drilling process. Geothermics, 15(No.1), (1986), pp. 17-22.

Williams, R. E. et al.: Advancements in Thermal Spallation Drilling Technology, Los Alamos: Los Alamos National Laboratory, (1988).

Worley, W. G.: Dissolution kinetics and mechanisms in quartz and granite water systems, Doctoral Thesis. Cambridge(Massachusetts): Massachusetts Institute of Technology, (1994).